Nonlinear Dyn (2017) 88:223–237
DOI 10.1007/s11071-016-3239-6

ORIGINAL PAPER

An effective numerical method for calculating nonlinear dynamics of structures with dry friction: application to predict the vibration response of blades with underplatform dampers

Dayi Zhang · Jianwei Fu · Qicheng Zhang · Jie Hong

Received: 7 June 2016 / Accepted: 23 November 2016 / Published online: 2 December 2016

Abstract This paper describes an efficient method to predict the nonlinear steady-state response of a complex structure with multi-scattered friction contacts. The contact friction force is equivalent to additional stiffness and damping based on optimal approximation theory, and as a consequence, the computation is simplified greatly by the linearization for a nonlinear system. In order to obtain accurate pressure distribution on the contact interfaces, the dynamic contact normal pressure is obtained by the equivalent static analysis which is validated for most engineering cases. Considering the complex procedure to determine the transformation between two different contact states, the differential forms of friction force are given to solve the tangential force accurately under the complex movement of interfaces. The approaches developed in this paper are particularly suitable to solve the dynamic response of large-scale structures with local contact nonlinearities. The entire procedure to calculate the steady-state response of a finite element model with a large number of degrees of freedom is demonstrated taking the blades with underplatform dampers as an example. The method is proved to be accurate and efficient; in particular, it does not suffer convergence problem in the allowable range of precision error, which exhibits remarkable potential engineering application values.

Keywords Dry friction · Equivalent stiffness and damping · Underplatform damper · Nonlinear dynamics

D. Zhang (✉)· J. Fu · Q. Zhang · J. Hong
School of Energy and Power Engineering, Beihang University, No. 37 Xueyuan RD. Haidian Dist., Beijing 100191, People's Republic of China
e-mail: dayi@buaa.edu.cn

J. Hong
Collaborative Innovation Center of Advanced Aero-Engine, No. 37 Xueyuan RD. Haidian Dist., Beijing 100191, People's Republic of China

1 Introduction

Compared to linear systems which are currently well described by finite element method (FEM), the prediction for the nonlinear dynamic response of structures with contact interfaces [1] is a much more difficult issue, in particular for the complex structures with several interfaces, owning to complex and non-smooth mathematic descriptions of the contact behavior at the interfaces related the non-penetration condition and the constitutive equations to describe the friction [2]. A large number of dry friction models have been proposed to obtain complicated motion modality and to describe the nonlinear behavior due to contact and friction [3,4]; however, these methods are still difficult to be used to analyze actual structures with contact and friction [5] for most cases because of the complex contact states of interfaces and the large number of degrees of freedom (DOFs).

In order to describe the mechanical behavior at contact surface, the node-to-node contact elements [6] are used in contact dynamic calculation, so that the relation between contact force and state of motion of the system can be clearly expressed. For the sake of simplification of complex contact models, the lumped parameter system with each contact surface reduced to one contact element [6,7] is often used to study the properties of structures, and the complex nonlinear phenomenon can be observed due to dry friction. However, the distribution of contact force, to a great extent, may affect the dynamic performance of the systems. As a result, multi-contact elements are presented to better simulate the contact surfaces [8,9].

When contact elements are used for a complex system composed of large amount of DOFs, it is unpractical to acquire the steady-state solution by direct time integration (DTI) in time domain, on account of the unbearable amount of calculation. Therefore, the harmonic balance method (HBM), as an approximate but highly efficient optional solution method in frequency domain, is widely used in the dynamical simulation for systems with friction contacts [10,11]. In steady-state dynamic response calculation, the transformation from nonlinear to linear system can greatly reduce computational costs, by making the contact force equivalent to additional linear constraints in terms of the averaging additional stiffness and damping. The additional stiffness and damping can be calculated by employed Fourier series expansion to divide the induced periodic friction force into the combination of displacement and velocity [12].

In the present paper, the nonlinear contact force is substituted by additional linear stiffness and damping based on optimal approximation theory; consequently, the steady-state response of the system can be solved by linearization of the nonlinear differential equation using the multi-harmonic balance method (MHBM). In complex mechanical systems, the differential forms of friction force described by relative displacement and time are derived to calculate the tangential force with great precision by integration. Considering the complexity of surface-to-surface contact, the quasi-static state condition is given to calculate the normal pressure distribution in the dynamic calculation. These methods are applied to calculate the dynamic response of a mass on a vibrational foundation and to predict the blade vibration with under-platform dampers.

2 Governing equations of a system with contact surfaces

2.1 Governing equations

The dynamic of a spatially discrete mechanical system with contact surfaces is governed by a second-order ordinary differential equation,

$$M\ddot{u}(t) + C\dot{u}(t) + Ku(t) = F(t) + F_c(t, u(t), \dot{u}(t)) \tag{1}$$

Herein, M, C and K are the matrices for the mass, the linear viscous damping and the stiffness, respectively. $F_c(t)$ and $F(t)$ are the vectors for the external force and the contact force acting on the contact interface. $u(t)$ is the vector of generalized displacements. In the case of periodical external excitation, the steady-state solution $u(t)$ and external force can be expressed in the form of a truncated series of harmonic terms,

$$F(t) = f_0 + \mathrm{Re}\left(\sum_{k=1}^{k=n} f(\omega_k)\mathrm{e}^{j(\omega_k t+\phi_{fk})}\right) \tag{2}$$

$$u(t) = q_0 + \mathrm{Re}\left(\sum_{k=1}^{k=n} q(\omega_k)\mathrm{e}^{j(\omega_k t+\phi_{uk})}\right) \tag{3}$$

where f_0 and q_0 are the vectors for the static components of the external force and the displacement, respectively; ω_k is the main component of circular frequencies; and ϕ_{fk} and $f(\omega_k)$ are the phase and amplitude at the frequency ω_k for the external force. Similarly, ϕ_{uk} and $q(\omega_k)$ are the phase and amplitude of generalized coordinates at frequency ω_k for the displacement.

For a system with stable periodic vibration, all the excitation force applied to the system must be periodical. Accordingly, the contact forces can be expressed as a function of $u(t)$ and $\dot{u}(t)$ in a whole stable vibration cycle. Without loss of generality, nonlinear contact force can be represented as an approximately linear combination of $u(t)$ and $\dot{u}(t)$.

$$F_c(u(t), \dot{u}(t)) = K_{\mathrm{ad}}(t)u(t) + C_{\mathrm{ad}}(t)\dot{u}(t) + F_{c0} \tag{4}$$

where F_{c0} is the constant part of the contact force and $K_{\mathrm{ad}}(t)$ and $C_{\mathrm{ad}}(t)$ are the time-varying additional equivalent stiffness and damping of the normal pressure and friction acting on the contact surface, respectively. By inserting Eq. (4) into (1), the equivalent form of the nonlinear differential equation is obtained.

$$M\ddot{u}(t) + (C - C_{\mathrm{ad}}(t))\dot{u}(t) + (K - K_{\mathrm{ad}}(t))u(t) = F(t) + F_{c0} \tag{5}$$

here by substituting external force $F(t)$ using Eq. (2) and generalized displacements $u(t)$ using Eq. (3), the set of nonlinear differential balance Eq. (5) is transformed into a set of nonlinear algebraic equations.

$$\begin{cases} (K - K_{\mathrm{ad}})q_0 = f_0 + F_{c0} \\ \left[-\omega_k^2 M + i\omega_k \left(C - C'_{\mathrm{ad}}(q, \omega_k)\right) \right. \\ \left. + \left(K - K'_{\mathrm{ad}}(q, \omega_k)\right)\right] q(\omega_k) \mathrm{e}^{j\phi_{uk}} = f(\omega_k)\mathrm{e}^{j\phi_{fk}} \\ \text{with} \quad k = 1, \ldots, n \end{cases} \tag{6}$$

Supposing that the additional equivalent stiffness $K_{\mathrm{ad}}(t)$ and the damping $C_{\mathrm{ad}}(t)$ show a weak correlation with time t, the average additional stiffness and damping can be used in Eq. (6) by substituting the time-varying additional equivalent stiffness and damping. And as a consequence, we obtain the approximate linearization of the nonlinear algebraic Eq. (6), which makes it more efficient and convenient to solve these equations. In most cases, the approximate solution is more efficient and with sufficient accuracy for practical applications.

2.2 The optimal approximation of contact force

For most of the discrete mechanical structures related to finite element method, there are only a small part of nodes involved in the contact surface if compared with the whole structure. Therefore, it is not difficult to get the contact force for a given displacement of the contacted nodes. Then, the time-varying additional equivalent stiffness $K_{\mathrm{ad}}(t)$ and damping $C_{\mathrm{ad}}(t)$ should be calculated to solve the nonlinear algebraic Eq. (6). On condition that the average additional stiffness and damping are used to approximately express the contact force, Eq. (4) can be rewritten as the following equation,

$$F_c(u(t), \dot{u}(t)) \approx K_{\mathrm{ad}}^0 u(t) + C_{\mathrm{ad}}^0 \dot{u}(t) + F_{c0} \tag{7}$$

where K_{ad}^0 and C_{ad}^0 are the average additional stiffness and damping, whose values are constant. As we can see from Eq. (7), the solution of K_{ad}^0 and C_{ad}^0 can be transformed into the solution of combinatorial coefficient of $u(t)$ and $\dot{u}(t)$ which makes the right-hand side of the equation becomes the best approximation of the contact force. At present, the most common estimation method is least-squares function approximation, and the idea behind least-square approach is to minimize the difference between the original function and the approximation. The difference can be measured by the error function over the interval $[0\ T]$, which is defined by:

$$\prod(t) = \int_0^T \left(F_c(t) - K_{\mathrm{ad}}^0 u(t) - C_{\mathrm{ad}}^0 \dot{u}(t) - F_{c0}\right)^2 \mathrm{d}t \tag{8}$$

where T is the period of vibration, which satisfies the condition $u(t) = u(t+T)$ and $F_c(t) = F_c(t+T)$. $u(t)$ and $\dot{u}(t)$ are mutually orthogonal, which means they satisfy Eq. (9).

$$\int_0^T u(t)\dot{u}(t)\mathrm{d}t = \int_0^T u(t)\mathrm{d}u(t) = \frac{1}{2}u(t)^2|_0^T = 0 \tag{9}$$

The condition under which integral function $\prod(t)$ reaches its minimum value is that the first-order partial derivative of the function is zero, so we can derive,

$$\frac{\partial \prod(t)}{\partial F_{c0}} = 0, \quad \frac{\partial \prod(t)}{\partial K_{\mathrm{ad}}^0} = 0, \quad \frac{\partial \prod(t)}{\partial C_{\mathrm{ad}}^0} = 0 \tag{10}$$

By inserting Eq. (8) into (10), we obtain the solution of the averaging additional stiffness and damping, through solving the equation group (11).

$$\begin{cases} F_{c0} = \dfrac{\int_0^T F(t)\mathrm{d}t \int_0^T u^2(t)\mathrm{d}t - \int_0^T u(t)\mathrm{d}t \int_0^T u(t)F(t)\mathrm{d}t}{T\int_0^T u^2(t)\mathrm{d}t - \left(\int_0^T u(t)\mathrm{d}t\right)^2} \\ K_{\mathrm{ad}}^0 = \dfrac{\int_0^T F(t)\mathrm{d}t \int_0^T u(t)\mathrm{d}t - T\int_0^T u(t)F(t)\mathrm{d}t}{\left(\int_0^T u(t)\mathrm{d}t\right)^2 - T\int_0^T u^2(t)\mathrm{d}t} \\ C_{\mathrm{ad}}^0 = \dfrac{\int_0^T \dot{u}(t)F(t)\mathrm{d}t}{\int_0^T \dot{u}^2(t)\mathrm{d}t} \end{cases} \tag{11}$$

The work W_F done by the nonlinear force $F(t)$ and its approximation in a periodic vibration can be calculated by Eqs. (12) and (13), respectively,

$$W_F = \int_0^T F(t)\mathrm{d}u(t) = \int_0^T F(t)\dot{u}(t)\mathrm{d}t \tag{12}$$

$$\begin{aligned} W_{Fp} &= \int_0^T \left(K_{\mathrm{ad}}^0 u(t) + C_{\mathrm{ad}}^0 \dot{u}(t) + F_{c0}\right)\mathrm{d}u(t) \\ &= C_{\mathrm{ad}}^0 \int_0^T \dot{u}^2(t)\mathrm{d}t = \int_0^T F(t)\dot{u}(t)\mathrm{d}t = W_F \end{aligned} \tag{13}$$

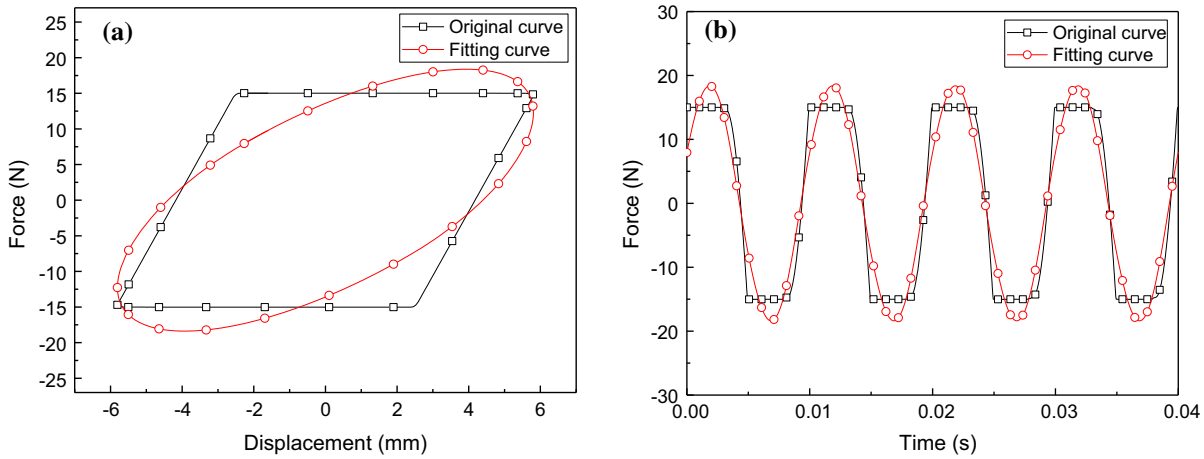

Fig. 1 An example of the original curve and its fitting curve **a** hysteresis loops and **b** in time domain

It can be concluded that the work done by the nonlinear force is equal to the work done by its approximation force in Eqs. (12) and (13). Without loss of generality, the nonlinear force $F(t)$ and the displacement $u(t)$ can be represented as Fourier series.

$$\begin{cases} F_c(t) = f_0 + \sum_{k=1}^{n} \left(f_{\mathrm{sk}} \sin(k\omega t) + f_{\mathrm{ck}} \cos(k\omega t)\right) \\ u(t) = \sum_{k=1}^{n} \left(a_k \sin(k\omega t) + b_k \cos(k\omega t)\right) \end{cases} \tag{14}$$

where ω is the angular velocity, and the period of vibration T can be expressed as $2\pi/\omega$. f_0 is the static component of the nonlinear force; f_{sk}, f_{ck} and a_k, b_k are the harmonic components of $F_c(t)$ and $u(t)$, respectively. The solution of the averaging additional stiffness and damping can be calculated by inserting Eq. (14) into (11), so we can derive,

$$F_{c0} = f_0 \tag{15}$$

$$\begin{cases} K_{\mathrm{ad}}^0 = \dfrac{\int_0^T u(t)F(t)\mathrm{d}t}{\int_0^T u^2(t)\mathrm{d}t} = \dfrac{\sum_{k=1}^n (a_k f_{\mathrm{sk}} + b_k f_{\mathrm{ck}})}{\sum_{k=1}^n (a_k^2 + b_k^2)} \\ C_{\mathrm{ad}}^0 = \dfrac{\int_0^T \dot{u}(t)F(t)\mathrm{d}t}{\int_0^T \dot{u}^2(t)\mathrm{d}t} = \dfrac{\sum_{k=1}^n (a_k f_{\mathrm{ck}} - b_k f_{\mathrm{sk}})}{\sum_{k=1}^n k\omega(a_k^2 + b_k^2)} \end{cases} \tag{16}$$

As exhibited by Eq. (16), the averaging additional stiffness is the equivalent average value of each harmonic component of stiffness, which also goes for the additional damping. In the case that only the first harmonic component of the displacement is reserved, we will obtain the same expressions for the additional stiffness and damping which are given in Ref. [12].

An example of two-slope hysteresis curve and its fitting curve are shown in Fig. 1a, and the fitting curve is calculated using Eq. (11) in time domain. As shown in Fig. 1a, b, the fitting curve does not guarantee the force to be equal to its original value at every point, but the minimum of square error is achieved between the original data and fitting data in one cycle of oscillation.

3 Contact modeling

3.1 Node-to-node contact element

In order to derive the expression of contact forces $F_c(u(t), \dot{u}(t))$ in Eq. (5) acting on the contact surfaces, the node-to-node contact element [12–14] (Fig. 2) is widely used to model contact force. Normal contact stiffness k_n is defined to establish a relationship between normal force and relative displacement in the normal direction on the contact surface; then, expressions for normal force can be derived in the following form,

$$N = \begin{cases} k_n(z_2 - z_1) = k_n g_n & \text{for contact} \\ 0 & \text{for separation} \end{cases} \tag{17}$$

Herein, z_1 and z_2 are the normal displacements for the two contact nodes, respectively. Thus, g_n defines the magnitude of penetration of one body into the other at the contact node.

In order to describe the dependence of friction force and tangential relative displacement and velocity on the contact interface, a series of frictional models are developed in the last few decades. Coulomb friction model

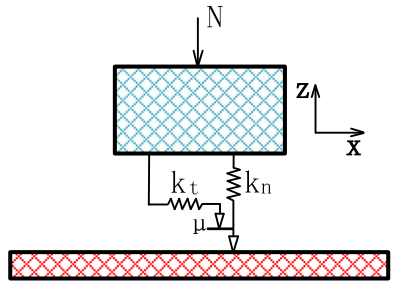

Fig. 2 Node-to-node contact element

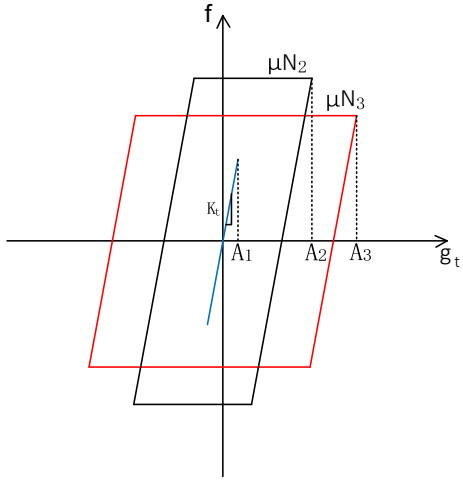

Fig. 3 Two-slope hysteresis friction model

[15], Dahl model [16] and LuGre model [17] are the approximate descriptions for the dynamic of friction force under different operating conditions. Two-slope hysteresis friction model (Fig. 3) is widely applied in the analysis of various nonlinear systems [13,18,19], because of its intuitive physical meanings and numerical advantages in engineering. As a tiny tangential force acting on a body, only the elastic deformation occurred on the contact surface without relative displacement between contact nodes on the interface, which is called stick stage. When the tangential force exceed the critical value μN, where μ is the coefficient of friction, the sliding occurs on the contact surface and the friction force remains constant.

As shown in Fig. 2, the value of the tangential force relays on the contact state. The integral form of the friction force is defined as,

$$f = \begin{cases} k_t(x_2 - x_1) = k_t g_t & \text{for stick} \\ \mu N \text{sgn}(\dot{x}_2 - \dot{x}_1) = \mu N \text{sgn}(\dot{g}_t) & \text{for slip} \\ 0 & \text{for separation} \end{cases} \tag{18}$$

where x_2 and x_1 are the tangential displacements of respective contact nodes. Thus, g_t denotes the relative tangential displacement on the interface.

As illustrated in Eq. (18), friction force is equal to 0 when $x_2 = x_1$, which shows this formula is valid at reciprocating vibration near the equilibrium point. On condition that the equilibrium point changes in the moving process, new contact element should be recreated. The determination of the state transition time is critical for friction calculation. The literature [13,20] has given an analytical criteria based on friction contact model to determine the transformation among stick, slip and separation of the friction contact. However, complex formulas must be calculated to determine the transformation between two different contact states, resulting from the different types of combinations of normal movement and tangential movement. To simplify the calculation of contact frictions, it is convenient to denote the friction force in a differential form with respect to the relative displacement, as shown in Eq. (19).

$$\begin{aligned} \frac{\mathrm{d}f(g_t, \dot{g}_t)}{\mathrm{d}g_t} &= -k_t H(\mu N - |f|) \\ &\quad - \left(\frac{1}{\mathrm{d}g_t}\right) H(|f| - \mu N)\,|\mu N - |f||\,\text{sgn}(f) \end{aligned} \tag{19}$$

where $H(\cdot)$ is a discontinuous function called Heaviside step function and can be written as,

$$H(x) = \begin{cases} 0, & x \le 0 \\ 1, & x > 0 \end{cases} \tag{20}$$

Moreover, the differential form of friction force with respect to time can be derived by using Eq. (19). As we can see from Eq. (19), the incremental form of friction makes it convenient to calculate friction force through integral in time domain without ignoring the changes in normal pressure which has a great influence on the friction force.

$$\begin{cases} \frac{\mathrm{d}f(g_t,\dot{g}_t)}{\mathrm{d}t} = \frac{\mathrm{d}f(g_t,\dot{g}_t)}{\mathrm{d}g_t}\frac{\mathrm{d}g_t}{\mathrm{d}t} \\ \frac{\mathrm{d}f(g_t,\dot{g}_t)}{\mathrm{d}t} = -k_t\dot{g}_t H(\mu N - |f|) \\ \quad -\left(\frac{1}{\mathrm{d}t}\right) H(|f| - \mu N)\,|\mu N - |f||\,\text{sgn}(f) \end{cases} \tag{21}$$

Given a fluctuant normal force and relative tangential displacement described in Eq. (21), the hysteresis loop of friction force can be investigated by numerical Runge–Kutta method, as shown in Fig. 4. Because of the fluctuation of normal load, the hysteresis loop

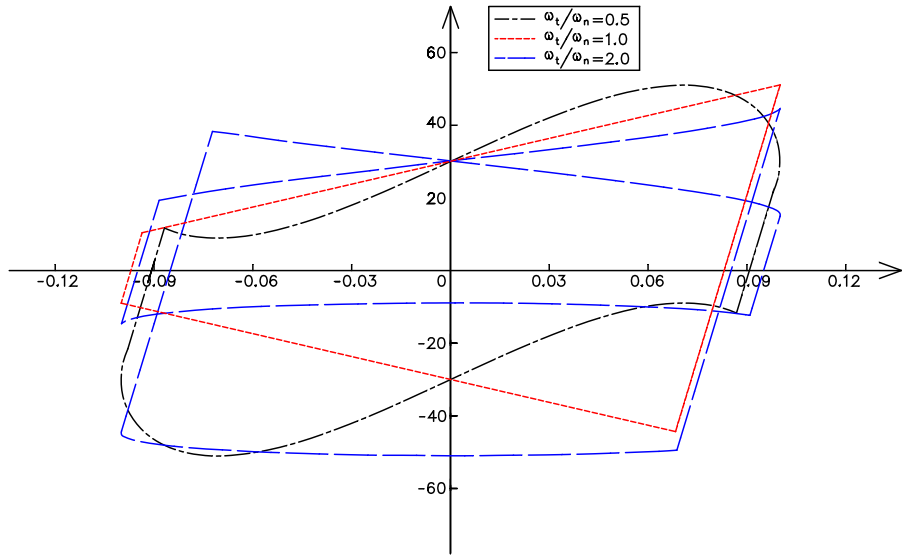

Fig. 4 Coupled vibration hysteresis loops

becomes much more complicated, even there are more than one open loop connected together to form a new hysteresis loop.

$$\begin{cases} N(t) = N_0 + N_1 \sin(\omega_n t) \\ g_t(t) = g_{t0} \sin(\omega_t t) \end{cases} \tag{22}$$

3.2 Surface-to-surface contact

It is always a challenge to analyze a structure with contact surfaces, owning to the complexity of contact calculation and the unacceptable computation time for large complex systems. In order to simplify that problem, the contact surface with dry friction is reduced to one contact element in some studies [21,22]. Moreover, many researchers [23–25] simulate the behavior of contact surfaces by creating discrete node-to-node contact elements at the interfaces in order that the distribution of contact force could be considered. According to the definition of stiffness, the normal contact stiffness for the contact elements can be calculated by Eq. (23).

$$k_{ni} = \frac{P_i}{u_{zi}} \quad (i = 1, 2, \ldots, n) \tag{23}$$

Herein, k_{ni} denotes the contact stiffness of the contact element i; P_i and u_{zi} are the normal force and the relative normal displacement, respectively, for the contact element i. As shown in Fig. 5, a rigid round punch with a flat base of diameter $2a$ is pressed into the frictionless surface of an elastic half-space, and the contact pressure distributions on the contact surface [26] is given by

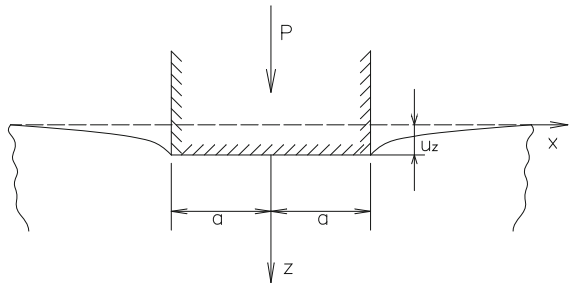

Fig. 5 Indention by a rigid plat punch

$$\begin{cases} p(x) = \frac{P}{(a^2 - x^2)^{1/2}} \\ u_z = \frac{\pi P}{E}(1 - \nu^2) \end{cases} \tag{24}$$

where E is Elastic modulus, and ν is Poisson's ratio.

Figure 6 shows an equivalent alternative model using discretized contact elements to simulate the contact in Fig. 5. By inserting Eq. (24) into (23), the normal contact stiffness can be written as the following expression equation.

$$k_n(x) = \frac{2Ex\Delta x}{(a^2 - x^2)^{1/2}(1 - \nu^2)} \tag{25}$$

Because there is no interaction between the contact elements of the model in Fig. 5, i.e., shear deformation between adjacent contact elements at the interface is ignored, so that the changing stiffness with respect to contact state in this model should be considered to coincide with practical results. Typically, the contact stiffness varies with contact surface geometry, relative position of contact interface and external load. There-

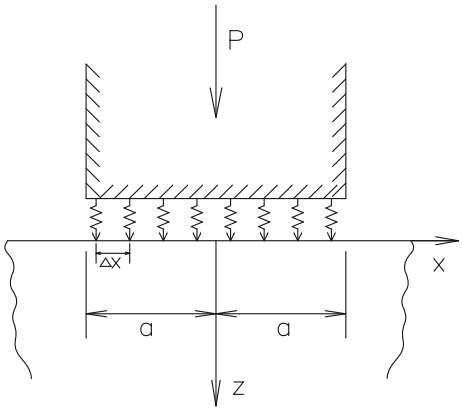

Fig. 6 Contact surface with discretized contact elements

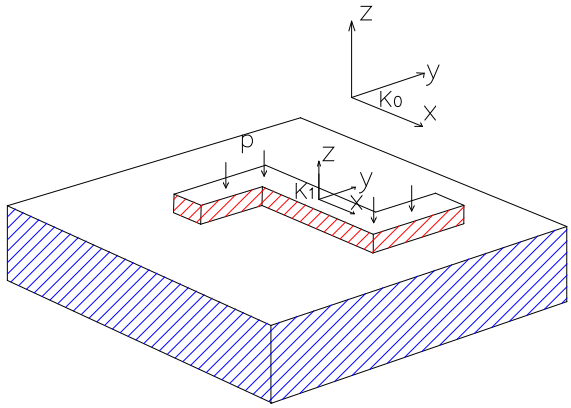

Fig. 7 Z-shape mass on a vibrational foundation

fore, it is difficult to obtain the precise distributions of contact stiffness allowing for unknown contact states, especially in dynamic calculations.

The dynamic contact problem can be treated as a static problem, on condition that the characteristic contact time T is much larger than the time that elastic waves in the continuum travel a distance on the order of contact area diameter D [27], which is also called the quasi-static state condition:

$$T > D/c \tag{26}$$

where c is the speed of sound. Taking steel for example, the sound propagation velocity in steel is about 5200 m/s. For a contact with $D = 1$ m, this condition is met for frequencies below approximately 5 kHz. Therefore, such assumption is reasonable for most contact problems. Assuming that the dependence between contact forces and contact statues (such as relative position and external force) is obtained by static analysis in advance, there is no need for iterative solution of contact force in dynamic calculations. In order to reduce the amount of calculation, only a few independent contact states most likely to occur in dynamic calculation should be solved by quasi-static analysis, and the contact force in intermediate contact states can be obtained through interpolation calculation.

4 A mass on a vibrational foundation

4.1 Solution method

Figure 7 shows the case for a Z-shape mass which is placed on a vibrational foundation under uniformly

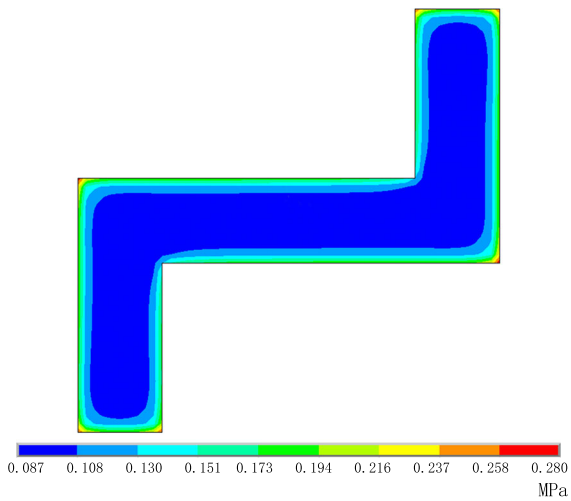

Fig. 8 Contact pressure distribution

distributed normal load on its top surface. A moving coordinate system K_1 fixed on the moving mass is used to describe the pressure distribution on the contact surface. Given a uniformly distributed pressure P_0, the contact pressure distribution is easily obtained by static analysis in ANSYS 15.0, as shown in Fig. 8.

As mentioned above, the normal pressure distribution depends on the relative position, the external force, etc. In this case, only external normal load and tangential inertial load are the factors affecting the distribution of pressure. Due to the small thickness of this mass compared with its length, the additional bending moment along the X- and Y-axes produced by inertial force is negligible; then, the additional normal con-

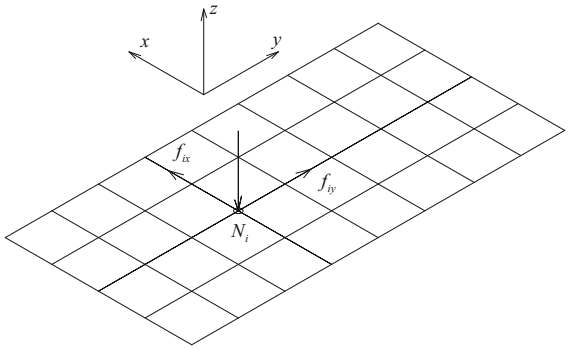

Fig. 9 Contact surface with discrete contact points

tact force used to balance the bending moment is also negligible. If the two contact surfaces had the same elastic parameters, any tangential traction transmitted between them gives rise to equal and opposite normal displacements of every point on the contact surface. Consequently, the two bending contact surfaces conform exactly with each other, and the distribution of normal pressure is not disturbed. The shape and size of the contact area are fixed by the profiles of the two surfaces and normal force, and independent of the tangential force [26].

As shown in Fig. 7, the contact is the typical receding contact, where the loaded contact area is completely contained within the unloaded contact area. The receding contact has been shown by Dundurs [28] to have two special properties. Firstly, if the load increased in magnitude and its distribution did not change, the contact area will not change in shape or size, and secondly, the displacement, strain and stresses change linearly with the normal load. Therefore, the distribution of normal load on the contact surface can be derived by

$$N_p(x, y) = \frac{p}{p_0} N_{p_0}(x, y) \tag{27}$$

where $N_p(x, y)$ and $N_{p0}(x, y)$ are the normal pressure distribution with normal load p and p_0, respectively. In order to describe the normal pressure distribution on the contact surface, the interface is discretized into a set of contact points, shown in Fig. 9 by the points of crossing.

Considering the distribution of normal and tangential force on the contact surface, the dynamic equations of the mass on a vibrational foundation can be derived by using D'Alambert's principle.

$$\begin{cases} m\ddot{x} = \sum_{i=1}^{n} f_{ix} \\ m\ddot{y} = \sum_{i=1}^{n} f_{iy} \\ I\ddot{\theta} = -\sum_{i=1}^{n} f_{ix} y_i^1 + \sum_{i=1}^{n} f_{iy} x_i^1 \\ \frac{\mathrm{d}f_{ix}}{\mathrm{d}t} = -k_{it}\dot{g}_{txi} H(f_{x\max i} - |f_{ix}|) - \left(\frac{1}{\mathrm{d}t}\right) \\ H(f_{ix} - f_{x\max i})\,|f_{x\max i} - |f_{ix}||\,\mathrm{sgn}(f_{ix}) \\ \frac{\mathrm{d}f_{iy}}{\mathrm{d}t} = -k_{it}\dot{g}_{tyi} H(f_{y\max i} - |f_{iy}|) - \left(\frac{1}{\mathrm{d}t}\right) \\ H(f_{iy} - f_{y\max i})\,|f_{y\max i} - |f_{iy}||\,\mathrm{sgn}(f_{iy}) \end{cases} \tag{28}$$

where m and I are the mass and the moment of inertia for Z-axis, respectively; x and y are two translational degrees of freedom in yz plane of global coordinate system K_0; θ is the rotational degree of freedom along the z-axis; x_i^1, y_i^1 are the coordinates of node i on the discrete contact surface in the moving coordinate system K_1; f_{ix}, f_{iy} are the friction force; and $\dot{g}_{txi}$, $\dot{g}_{tyi}$ are the relative tangential velocity of node i in x and y directions, respectively. $f_{x\max i}$ and $f_{y\max i}$ are critical frictional force and can be given by Eq. (29).

$$\begin{cases} f_{x\max i} = \sqrt{\left(\mu \frac{p}{p_0} N_{0i}\right)^2 - f_{yi}^2} \\ f_{y\max i} = \sqrt{\left(\mu \frac{p}{p_0} N_{0i}\right)^2 - f_{xi}^2} \\ \dot{g}_{txi} = \dot{x}_i - \dot{x}_b - y_i^1 \dot{\theta} \\ \dot{g}_{tyi} = \dot{y}_i - \dot{y}_b + x_i^1 \dot{\theta} \end{cases} \tag{29}$$

Herein, N_{0i} denotes the normal load of node i on the contact surface; $\dot{x}_b$ and $\dot{y}_b$ is the vibration velocity of the foundation in the global coordinate system. In Eq. (28), the derivative of friction force with respect to time is given, instead of using the constitutive equations in integral form, and it is capable of describing complex friction with high precision under various situations of different contact states.

Given a fluctuation of normal load $P(t)$ and foundation displacement $\dot{x}_b$ and $\dot{y}_b$ as shown in Eq. (30).

$$\begin{cases} P(t) = P_0 + P_1 \sin(2\pi f_p t) \\ x_b(t) = x_0 \sin(2\pi f_b t) \\ y_b(t) = 0 \end{cases} \tag{30}$$

Herein, f_b and f_p are the vibration frequency of the foundation and the normal load, and the relative displacement of the mass with respect to the foundation can be defined as:

$$\begin{Bmatrix} x_r \\ y_r \end{Bmatrix} = \begin{Bmatrix} x_b - x \\ y_b - y \end{Bmatrix} \tag{31}$$

Table 1 Parameters for the example

Parameter	Value	Parameter	Value
m	0.035 kg	μ	0.3
P_0	50 N	I	14.68e–6 kg m^2
P_1	30 N	x_0	0.005 m
f_b	100 Hz	f_p	0, 25, 50, 200 Hz

4.2 Results

The parameters of the system are given by Table 1, and it is easy to obtain the dynamic response of the mass by Time Domain Integration (TDI).

Hysteresis loops of friction force versus relative displacement are plotted together in Fig. 10 under different normal loads. Figure 10 shows that the shape of hysteresis loops are quite complex with fluctuations in normal load, rather than a normal bilinear hysteresis loop at constant normal load as shown in Fig. 10a. The shape of hysteresis loop depends on the ratio of frequency and phase lag between the horizontal displacement and the normal load vibration. As shown in Fig. 10a, b, there is only a complete hysteresis loop at the time when the frequency of normal load is an integral multiple of the foundation vibration frequency. However, when the frequency of foundation vibration are N times of normal load, the hysteresis loop is made up of N different open loops linked tighter end to end as shown in Fig. 10d, c. Moreover, it is not difficult to draw the conclusion that there is always an entire hysteresis loop on the condition that the frequency ratio for the normal load fluctuation over the foundation vibration is a rational number, and the number of open loops equals the

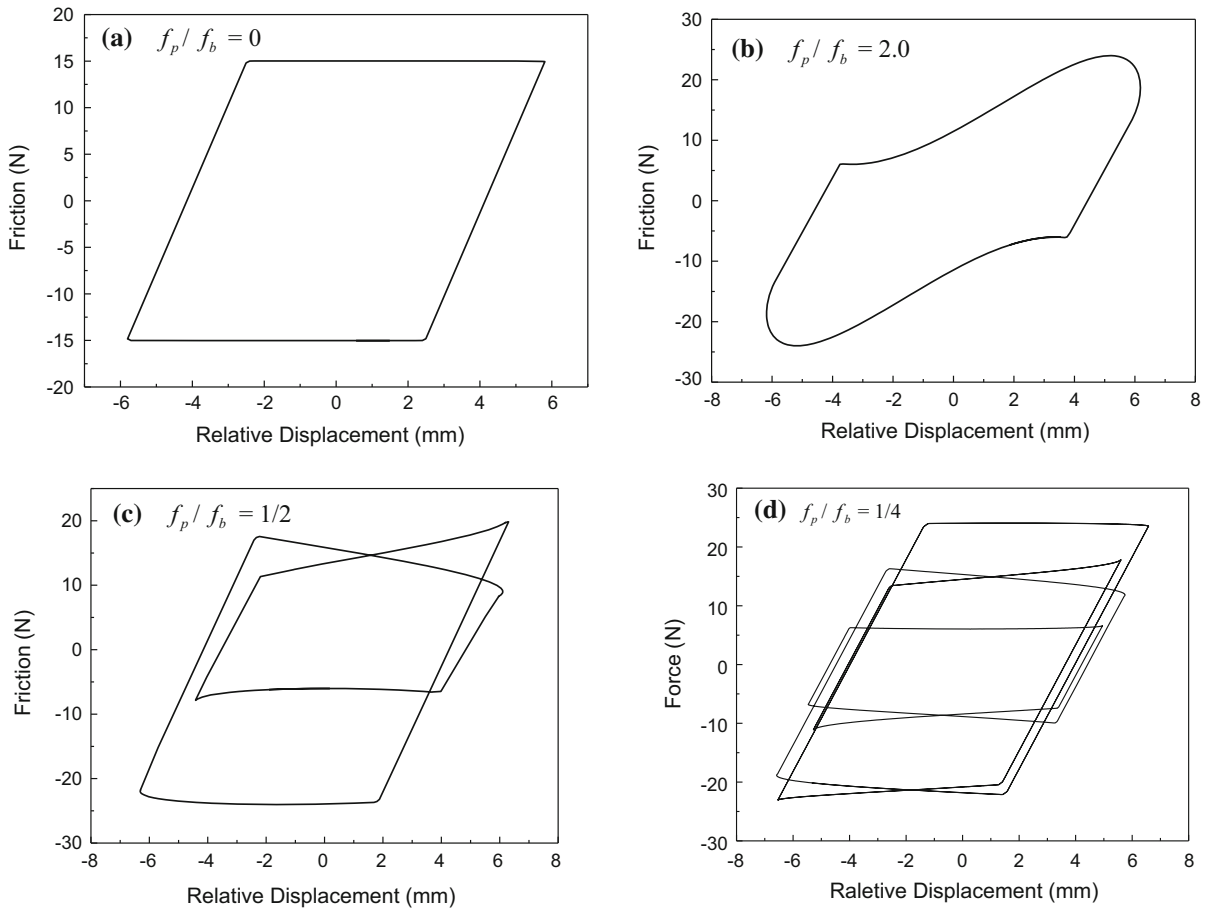

Fig. 10 Hysteresis loops for different frequency ratios

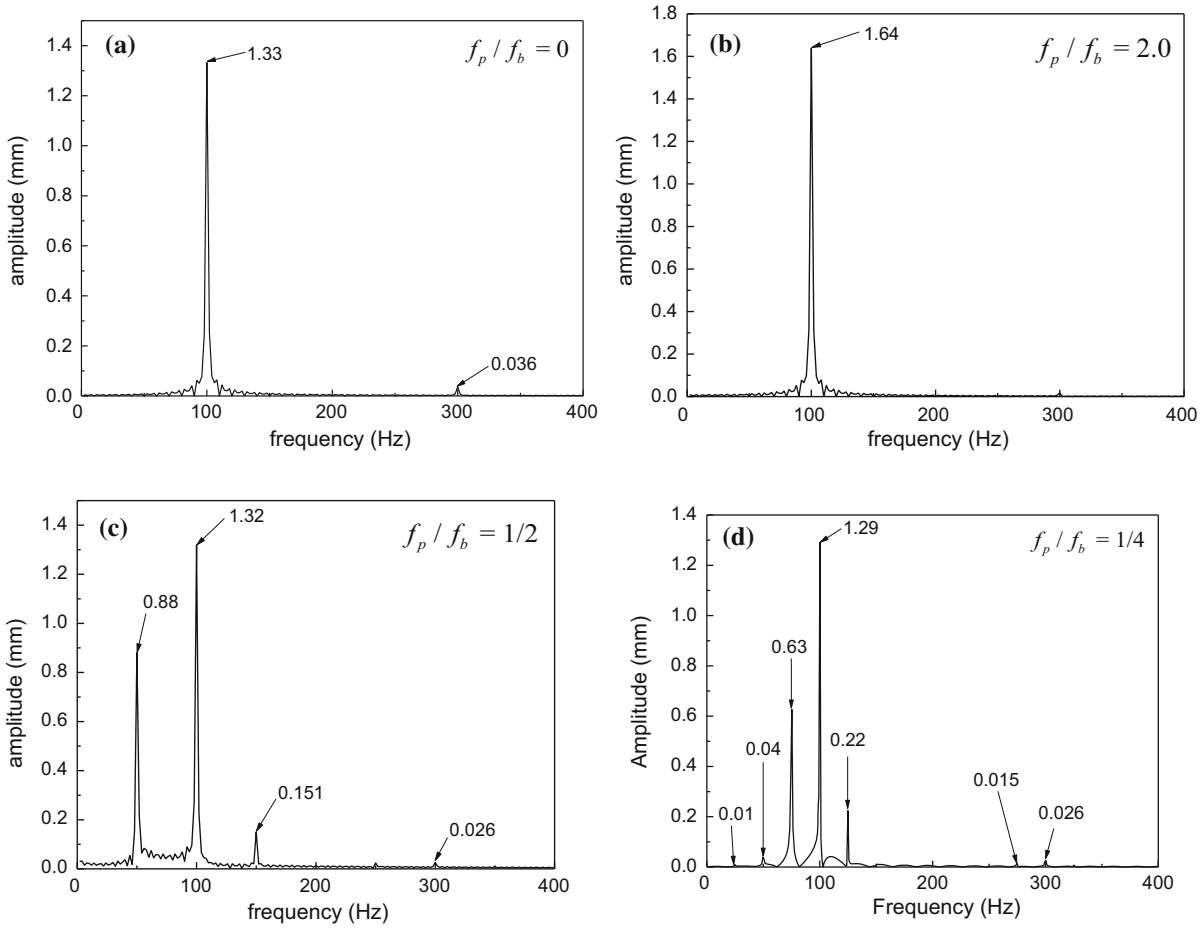

Fig. 11 FRFs of the mass for different frequency ratios

value of denominator of the frequency ratio which is reduced to its lowest terms.

The frequency response function (FRFs) of the mass is plotted in Fig. 11 at different normal loads. Friction force is the only driving force of the mass in horizontal direction, so that the shape of hysteresis loop determines the response of the mass. As shown in Fig. 10a–c, there is only one loop in an entire hysteresis loop. Thus, the vibrational energy is mainly concentrated on the dominant frequency. In the meantime, it is possible to see in Fig. 11a, b that the lower energy leakage on other frequencies will occur when the hysteresis loop is closer to an ellipse shape. However, in the case that the hysteresis loop contains more than one loop, the vibration energy is distributed in several different frequencies, such as the foundation and normal load vibration frequency, as is found in Fig. 11c, d.

5 Blades with underplatform dampers

5.1 Solution method

In order to demonstrate the applicability of the proposed method to more complex system, three plane blades with underplatform dampers are shown in Fig. 12a. In consideration of perfect cyclic symmetry, only a single blade and one damper with cyclic boundary condition are taken into account in the dynamic calculation, as shown in Fig. 12b. The condition of cyclic symmetry can be expressed by the equality relation of contact force between the blade and damper which can be written as:

$$F_{\mathrm{cd}}^{\mathrm{R}} = -F_{\mathrm{cb}}^{\mathrm{L}} \tag{32}$$

where $F_{\mathrm{cd}}^{\mathrm{R}}$ is the contact force on the right side of damper which is placed on the left side of the blade,

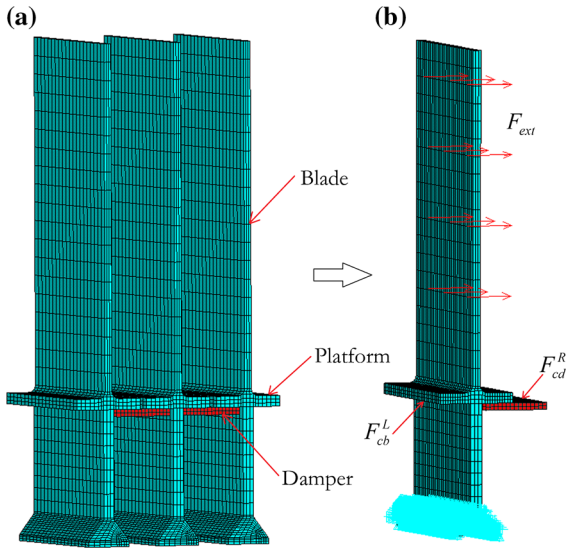

Fig. 12 Finite element model for the blades with dampers

and $F_{\mathrm{cb}}^{\mathrm{L}}$ denotes the contact force on the left side of the blade contact surface.

It is simple to analyze the nonlinear dynamic response of damper with only the DOFs on contact surfaces included, because there are fewer DOFs if compared with the whole system. A simplified dynamic model of damper without considering the local deformation is shown in Fig. 13. Supposing the vibration of platform is known in prior, the dynamic response of damper can be obtained by explicit dynamic analysis as discussed in Sect. 4.

The given assumption of the vibration of platform is used to obtain the dynamic response of damper. At the same time, the vibration between the damper and the platform interact; therefore, the iterative calculation is required to obtain the response of the blade. The flow chart for calculate the nonlinear vibration response of blades with underplatform dampers is shown in Fig. 14.

First of all, the response of blade without damper is calculated to obtain the stable response of platform by MHBM, and then, the nonlinear response of damper can be calculated by using DTI to obtain the contact force during a stable oscillating cycle. Next, the distribution of average additional stiffness and damper on the contact surface are calculated based on the theory of optimal approximation, and the stable response of blade with additional stiffness and damping will be solved once again by using MHBM. For a given response of platform u, a new response of platform u' will be obtained by one cycle of iteration. And the procedure can be represented by a function $g(u)$ in Eq. (33).

$$g(u) = u' \tag{33}$$

The discrete form of Newton method is used to determine the value of the next iteration and to accelerate the convergence of the iteration. According to the idea of discrete Newton method, the procedure of Newton can be written as:

$$\begin{cases} u_1 = g(u_0) \\ u_{k+1} = \frac{g(u_k)u_{k-1} - g(u_{k-1})u_k}{g(u_k) - u_k - g(u_{k-1}) + u_{k-1}} \quad (k > 1) \end{cases} \tag{34}$$

Herein, u_0 is the initial iterative value. In this iterative procedure, converge is achieved when the difference in platform response between two adjacent iterative calculations is smaller than a critical value. The convergence criteria can be expressed by

$$\|u_k - u_{k-1}\| < \varepsilon_u \|u_k\| \tag{35}$$

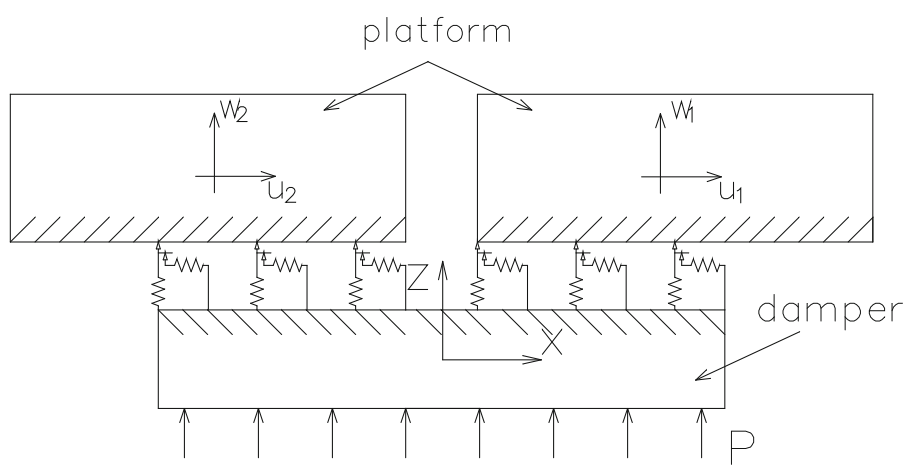

Fig. 13 Simplified model of the damper with contact interface

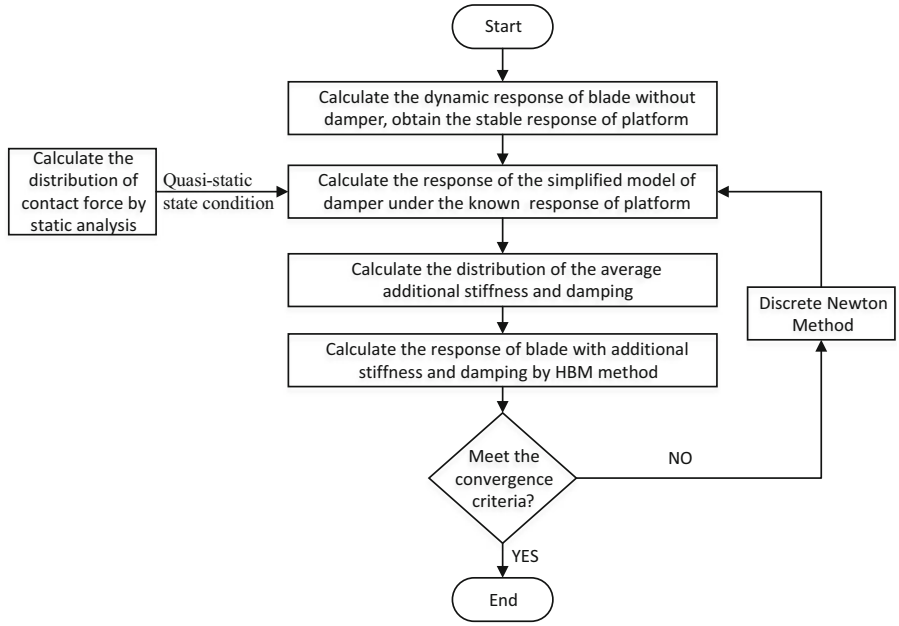

Fig. 14 Flow chart for calculating the nonlinear response of blade

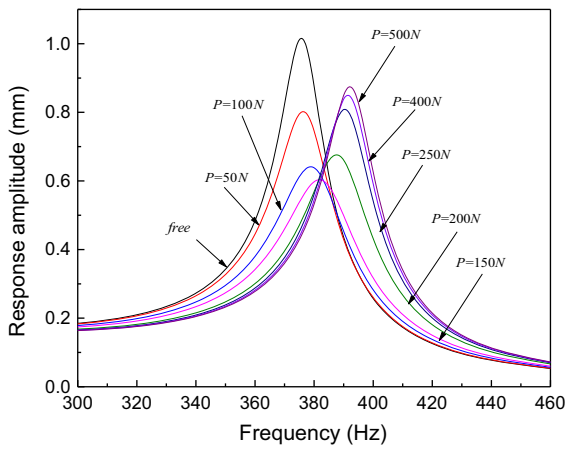

Fig. 15 FRFs for different normal loads ($m = 60\,\mathrm{g}$)

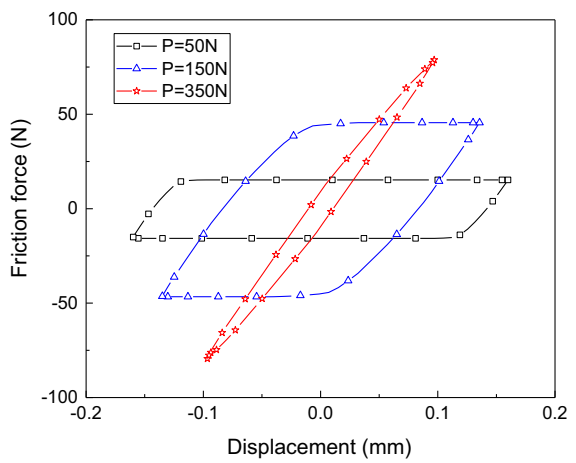

Fig. 16 Hysteresis loops for different amplitudes of normal load ($m = 60\,\mathrm{g}$)

where u_k and u_{k-1} are the response amplitude of platform in kth and $(k-1)$th iterative calculation. ε_u is the relative tolerance which is given by users.

As shown in Fig. 13, the dampers also vibrate slightly in normal direction during its horizontal vibration, which leads to a fluctuation of normal load. Due to the small vibration amplitude of platform, the normal load is large enough to prevent the separation between the contact surfaces. Compared to centrifugal load, the amplitude of normal load fluctuation is small, so that it does not affect the motion of damper in a great deal. The horizontal vibration of the damper is only required to consider in the kinetic calculation.

5.2 Results

The forced response of blades with underplatform dampers has been calculated using the above proposed method by giving a 2% convergence error. And the influence of normal load and damper weight on the nonlinear response of blade is investigated. The FRFs

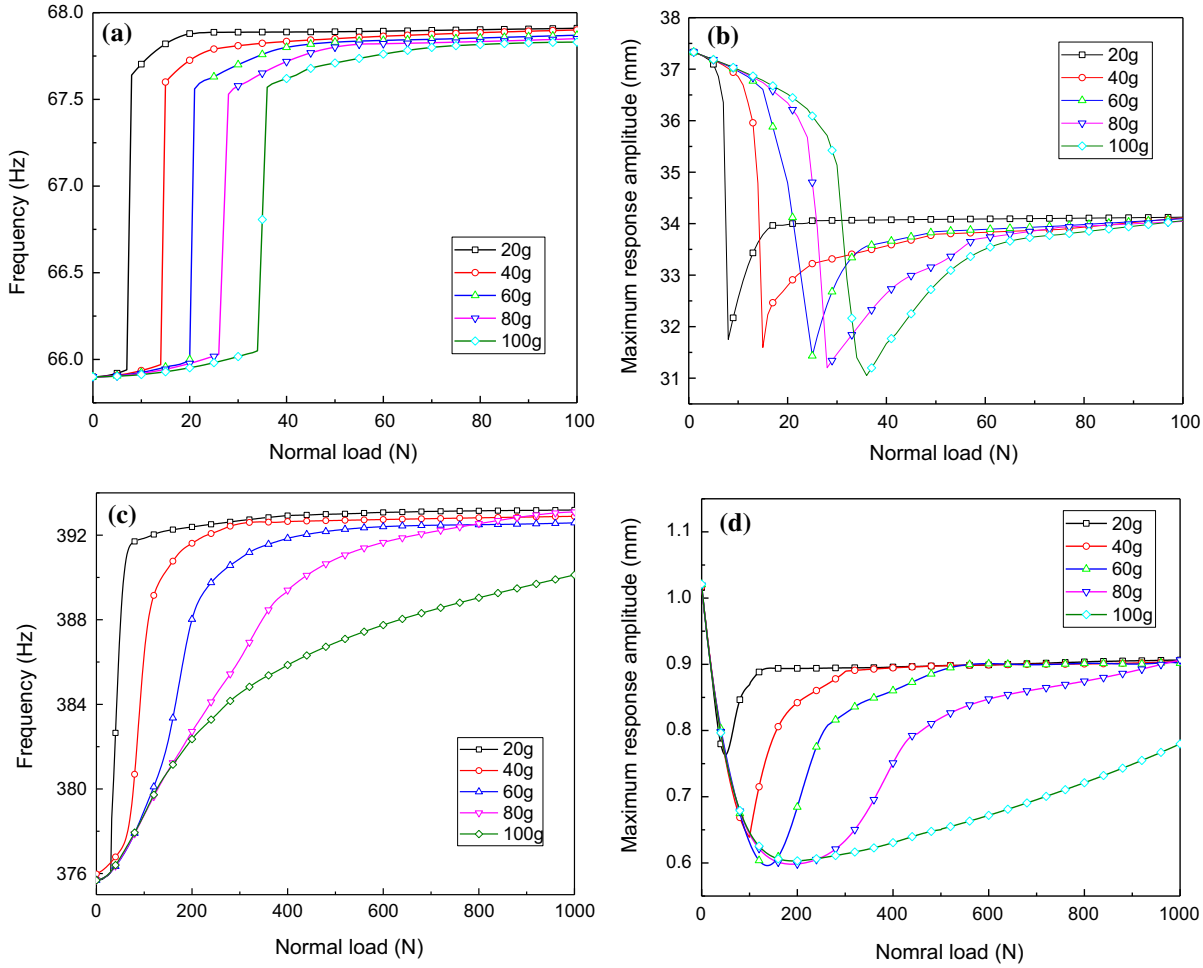

Fig. 17 Resonance frequency and amplitude with respect to normal loads for different weights of dampers, **a** the frequency and **b** the amplitude for the first-order resonance, **c** the frequency and **d** the amplitude for the second-order resonance

of the blades around the second modal frequency are plotted together in Fig. 15. The mass of the underplatform damper used in Fig. 15 is 60 g, and 8 different normal load amplitudes are applied in the simulation. It is obvious to see that the second-order resonant frequency increases gradually with the increment of normal load, while the resonant amplitude decreases firstly and then increases.

As shown in Fig. 16, the relative displacement of contact surfaces decreased and the friction force increased for the increasing of the normal loads. Consequently, the equivalent stiffness also increased which leads to the increment of the resonant frequency. When the normal load is greater than the critical value, the equivalent stiffness becomes equal to tangential stiffness of the contact surface in fully stick condition.

With a given weight of the damper, the percentage of sliding stage time over a period decreases with the increasing normal load. The dissipation of vibration energy occurs only in sliding state and can be calculated by the product of the friction force and the relative displacement. The equivalent damping of the friction force depends on the dissipated energy in one cycle of oscillation, i.e., the total area enclosed by the hysteresis curves. It is noticed that the enclosed area increases first and then decreases with increasing normal load which leads to corresponding behavior of the resonant amplitude shown in Fig. 16.

The first-order and second-order resonant frequency and amplitude with respect to normal loads for different weights of dampers are presented in Fig. 17. Figure 17b, d shows that there is always a normal load, called the optimal normal load, where the maximum response amplitude reaches its minimum value. On the vibrational foundation, the friction force on the damper in horizontal direction is balanced by the inertial force with a amplitude of $Am\omega^2$. Figure 17 also indicates that the stick state is more likely to happen when the ratio between the friction force and the inertial force is larger. Therefore, the larger mass of damper will lead to greater optimal normal load and smaller maximum response amplitude at the optimal normal load. Compared to the second-order resonant frequency, the first-order resonant frequency is much lower, resulting in smaller amplitude of inertial force, which makes the optimal normal load much smaller.

The transformation of contact state from sliding state to fully sticking state occurs within a narrow normal load range on condition of a small inertial force caused by low vibrational frequency or small mass damper with respect to normal load, as shown in Fig. 17. The sharp decrease in response amplitude near the optimal normal load leads to the steep increase in the equivalent stiffness, so that the jump phenomenon of resonant frequency is observed in Fig. 17a, c.

6 Conclusions

An effective numerical method to solve the nonlinear steady-state response of structures with multi-scattered friction contacts is achieved; both strict theoretical derivation and entire solution procedure by two intuitionistic cases study are given. The results for the nonlinear response of blades with underplatform dampers show that the resonant frequency increases and the resonant amplitude of blade decreases first and then increases for the increase in the normal load; the simulation results are coincident with previous studies by the other researchers to a great extent. The efficient method described in this paper gives an alternative choice to solve the dynamic problems of complex structures with multi-surface-to-surface contacts.

Acknowledgements This work was financially supported by the National Natural Science Foundation of China, the Grant Nos. 51475021 and 51575022.

References

1. Ma, H., Yin, F., Wu, Z., Tai, X., Wen, B.: Nonlinear vibration response analysis of a rotor-blade system with blade-tip rubbing. Nonlinear Dyn. **84**(3), 1225–1258 (2016)
2. Pennestrì, E., Rossi, V., Salvini, P., Valentini, P.P.: Review and comparison of dry friction force models. Nonlinear Dyn. **83**(4), 1785–1801 (2016)
3. Pascal, M.: Sticking and nonsticking orbits for a two-degree-of-freedom oscillator excited by dry friction and harmonic loading. Nonlinear Dyn. **77**(1), 267–276 (2014)
4. Jeffrey, M.R.: On the mathematical basis of solid friction. Nonlinear Dyn. **81**(4), 1699–1716 (2015)
5. Ma, H., Wang, D., Tai, X., Wen, B.: Vibration response analysis of blade-disk dovetail structure under blade tip rubbing condition. J. Vib. Control (2015). doi:10.1177/1077546315575835
6. Yang, B.D., Chu, M.L., Menq, C.H.: Stick-slip-separation analysis and non-linear stiffness and damping characterization of friction contacts having variable normal load. J. Sound Vib. **210**(4), 461–481 (1998)
7. Avalos, J., Mignolet, M.P.: On damping entire bladed disks through dampers on only a few blades. J. Eng. Gas Turbines Power **132**(9), 092503 (2010)
8. Laxalde, D., Thouverez, F., Lombard, J.P.: Forced response analysis of integrally bladed disks with friction ring dampers. J. Vib. Acoust. **132**(1), 011013 (2010)
9. Hohl, A., Siewert, C., Panning, L., Kayser, A.: Nonlinear vibration analysis of gas turbine bladings with shroud coupling. In: ASME Turbo Expo, vol. 5, pp. 425–433 (2008)
10. Zucca, S., Firrone, C.M.: Nonlinear dynamics of mechanical systems with friction contacts: coupled static and dynamic multi-harmonic balance method and multiple solutions. J. Sound Vib. **333**(3), 916–926 (2014)
11. Petrov, E.P.: Method for direct parametric analysis of nonlinear forced response of bladed discs with friction contact interfaces. In: ASME Turbo Expo, vol. 6, pp. 397–408 (2004)
12. Sanliturk, K.Y., Ewins, D.J.: Modelling two-dimensional friction contact and its application using harmonic balance method. J. Sound Vib. **193**(2), 511–523 (1996)
13. Petrov, E.P., Ewins, D.J.: Analytical formulation of friction interface elements for analysis of nonlinear multi-harmonic vibrations of bladed discs. In: ASME Turbo Expo, vol. 4, pp. 499–908 (2002)
14. Menq, C.H., Yang, B.D.: Non-linear spring resistance and friction damping of frictional constraint having two-dimensional motion. J. Sound Vib. **217**(1), 127–143 (1998)
15. Armstrong-Helouvry, B., Dupont, P., De Wit, C.C.: A survey of models, analysis tools, and compensation method for the control of machines with friction. Automatica **30**(7), 1083–1138 (1994)
16. Dahl, P.R.: A Solid Friction Model. The Aerospace Corporation, EL Segundo, CA (1986)
17. Hornstein, A.: Dynamical modeling with application to friction phenomena. Ph.D. thesis, Göttingen-Deutschland (2005)
18. Sanliturk, K.Y., Imregun, M., Ewins, D.J.: Harmonic balance vibration analysis of turbine blades with friction dampers. J. Vib. Acoust. **119**(1), 96–103 (1997)

19. Firrone, C.M., Zucca, S., Gola, M.: Effect of static/dynamic coupling on the forced response of turbine bladed disks with underplatform dampers. In: ASME Turbo Expo, vol. 6, pp. 429–440 (2009)
20. Chen, J.J., Yang, B.D., Menq, C.H.: Periodic forced response of structures having three-dimensional frictional constraints. J. Sound Vib. **229**(4), 775–792 (2000)
21. Ciğeroğlu, E., Özgüven, H.N.: Nonlinear vibration analysis of bladed disks with dry friction dampers. J. Sound Vib. **295**(3), 1028–1043 (2006)
22. Wang, A., Long, Q.: Forced response characteristics of bladed disks with mistuning non-linear friction. J. Cent. South Univ. **18**, 679–684 (2011)
23. Schwingshackl, C.W., Petrov, E.P., Ewins, D.J.: Effects of contact interface parameters on vibration of turbine bladed disks with underplatform dampers. J. Eng. Gas Turbines Power **134**(3), 032507 (2012)
24. Panning, L., Popp, K., Sextro, W., Götting, F., Kayser, A., Wolter, I.: Asymmetrical underplatform dampers in gas turbine bladings: theory and application. In: ASME Turbo Expo, vol. 6, pp. 269–280 (2004)
25. Zucca, S., Firrone, C.M., Gola, M.: Coupled static/dynamic modeling of wedge dampers for turbine blades. In: ASME Turbo Expo, vol. 6, pp. 1073–1086 (2010)
26. J Johnson, K.L.: Contact Mechanics. Cambridge University Press, Cambridge (1987)
27. Popov, V.L., Heß, M.: Method of Dimensionality Reduction in Contact Mechanics and Friction. Springer, Berlin (2015)
28. Dundurs, J.: Properties of elastic bodies in contact. In: de Pater, A.D., Kalker, J.J. (eds.) The Mechanics of the Contact Between Deformable Bodies, pp. 54–66. Delft University Press, Delft (1975)